Supporting Information

Investigation of excited state, reductive quenching, and intramolecular electron transfer of Ru(II)-Re(I) supramolecular photocatalysts for CO_2 reduction using time-resolved IR measurements

Kazuhide Koike,*[a] David C. Grills,[b] Yusuke Tamaki,[c] Etsuko Fujita,*[b] Kei Okubo,[c] Yasuomi Yamazaki, [c] Masaki Saigo,[d] Tatsuhiko Mukuta,[c] Ken Onda,[d] and Osamu Ishitani*[c]

[c]*National Institute of Advanced Industrial Science and Technology, 16-1 Onogawa, Tsukuba, Ibaraki, 305-8569, Japan*
[b]*Chemistry Division, Brookhaven National Laboratory, Upton, NY 11973-5000, USA*
[c]*Department of Chemistry, Tokyo Institute of Technology, O-okayama 2-12-1, E1-9, Meguro-ku, Tokyo 152-8550, Japan*
[d]*Department of Chemistry, Kyushu University, Fukuoka 819-0395, Japan.*

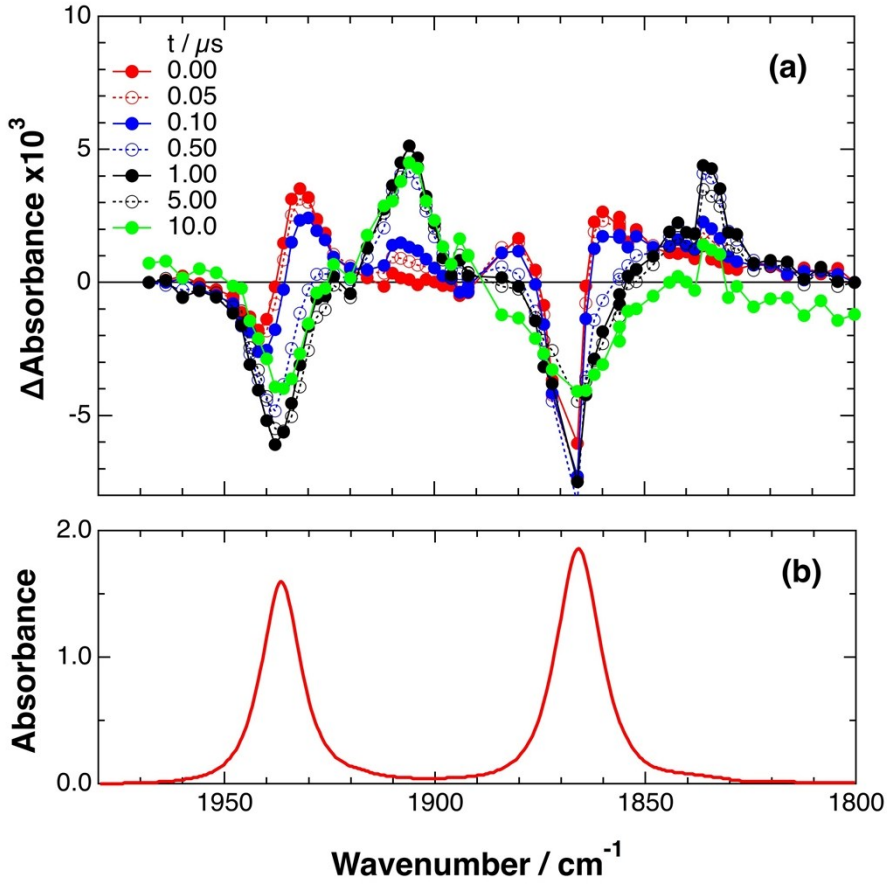

Fig. S1 (a) TRIR spectra recorded after 532 nm excitation of **RuRe(Ph)** in an argon-saturated CH_3CN solution. (b) FT-IR spectrum of **RuRe(Ph)** in CH_3CN.

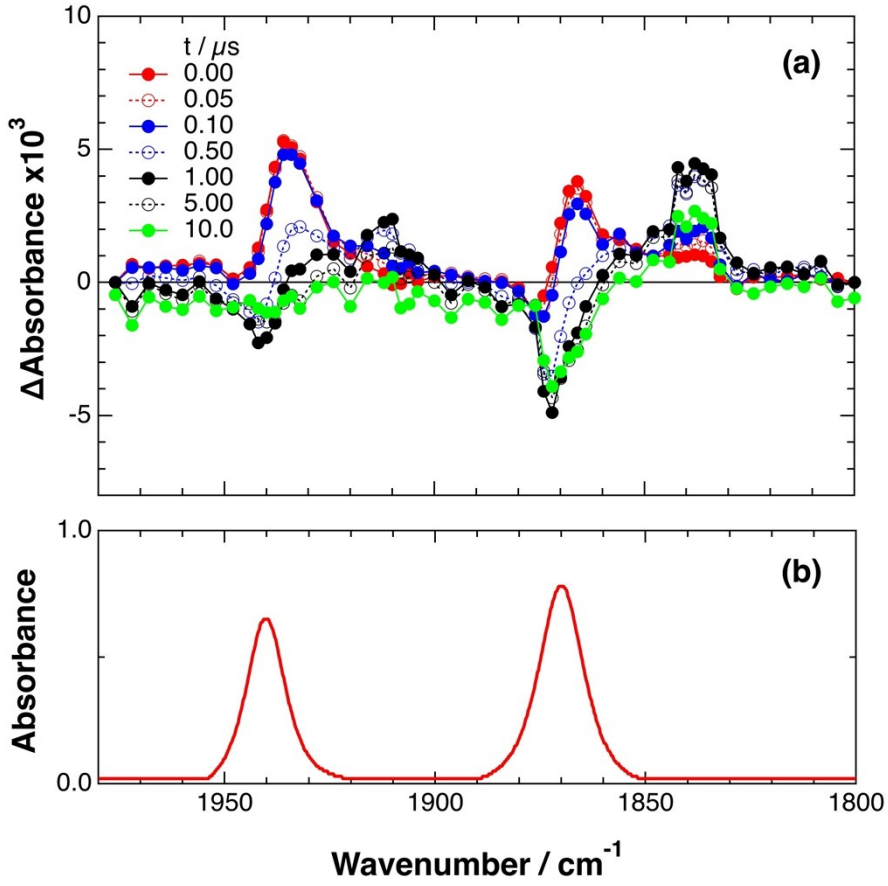

Fig. S2 (a) TRIR spectra recorded after 532 nm excitation of **RuRe(FPh)** in an argon-saturated CH_3CN solution. (b) FT-IR spectrum of **RuRe(FPh)** in CH_3CN.

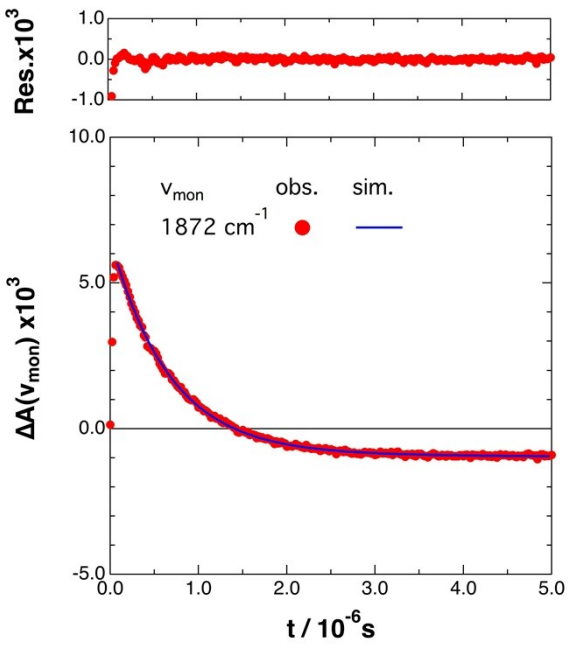

Fig. S3 Growth and decay of the transient infrared absorption bands of **RuRe(OEt)** in CH_3CN, monitored at 1872 cm^{-1} (•) after 532 nm excitation. The corresponding simulated absorbance change obtained from a triple exponential function with the same rate constants (k_{CS1}, k_{CS2} and k_{CR}) as eq. 8 is shown as a solid curve. Top panel shows the residual obtained from the simulation.

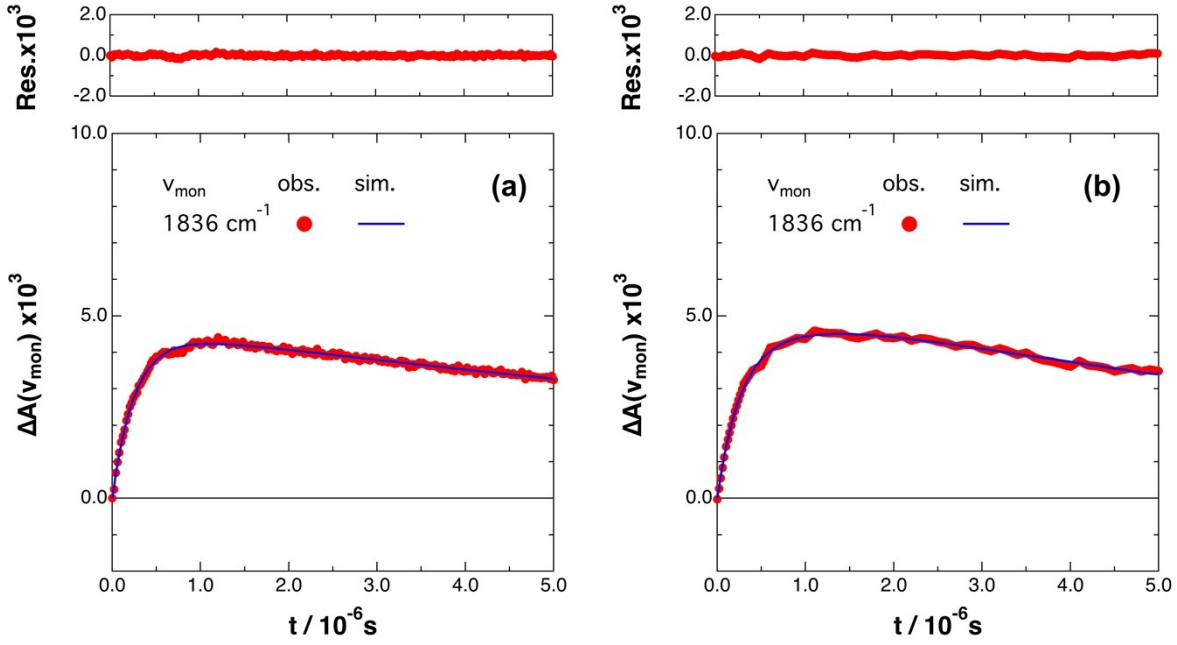

Fig. S4 Growth and decay of the transient infrared absorption bands of (a) **RuRe(Ph) and** (b) **RuRe(FPh)** in CH_3CN, monitored at 1836 cm^{-1} (•) after 532 nm excitation. The corresponding simulated absorbance changes obtained from eq. 8 are shown as solid curves. Top panel shows the residuals obtained from the simulations.

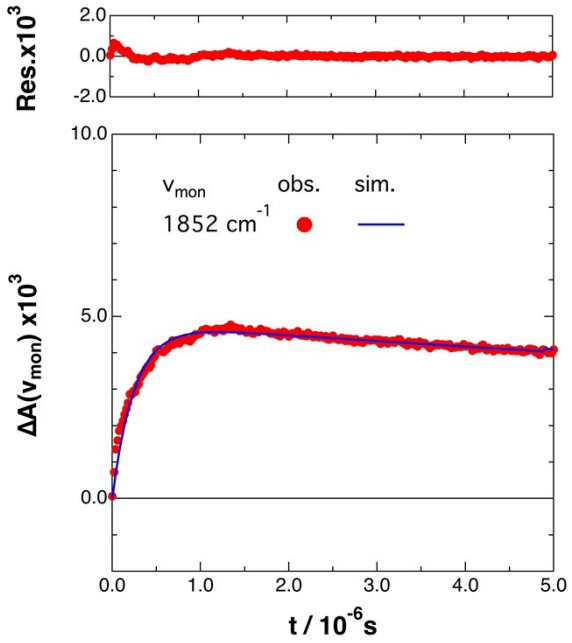

Fig. S5 Growth and decay of the transient infrared absorption bands of **RuRe(OEt)** in CH_3CN, monitored at 1852 cm^{-1} (•) after 532 nm excitation. The corresponding simulated absorbance change obtained from eq. 5 is shown as a solid curve. Top panel shows the residual obtained from the simulation.

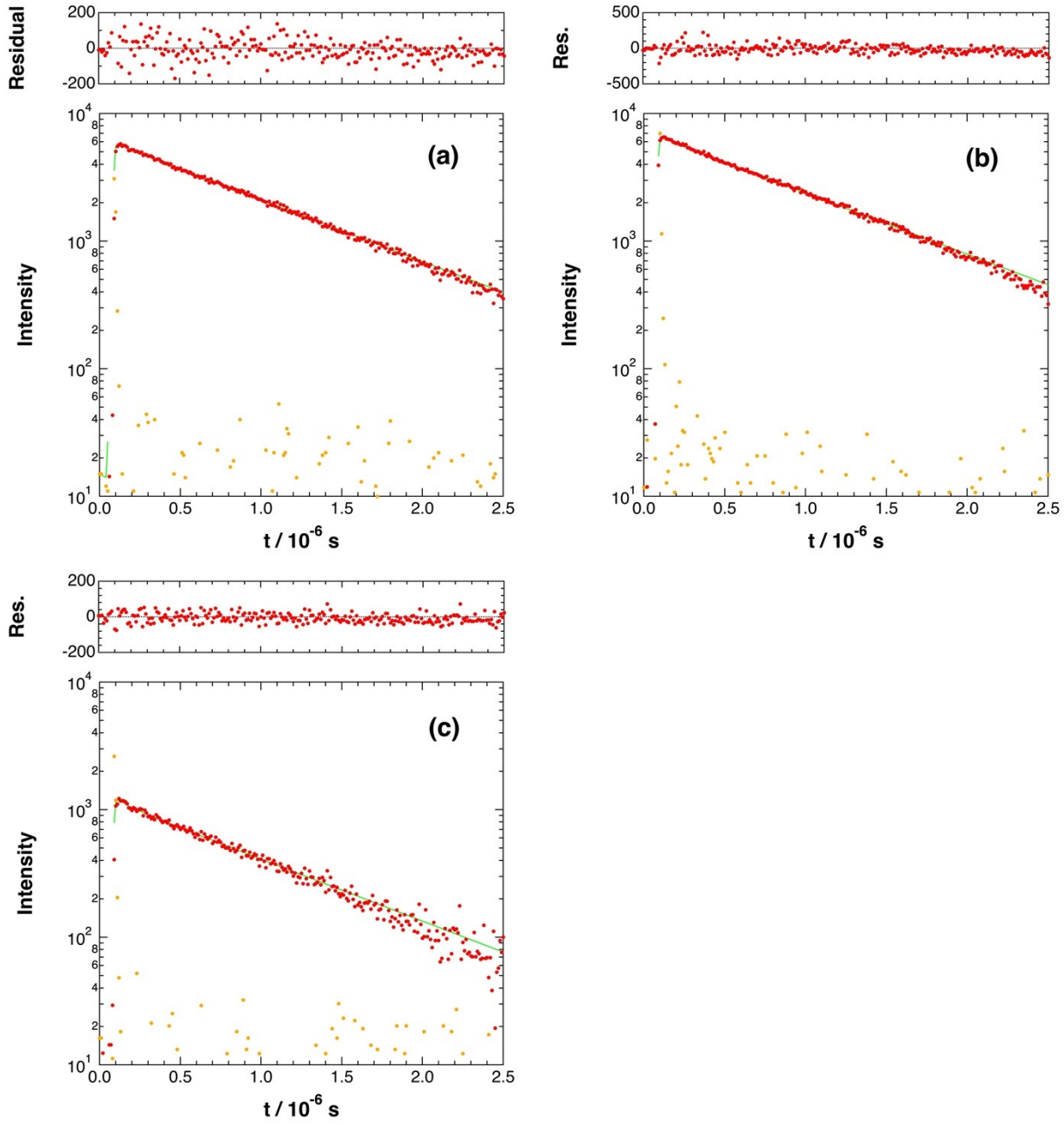

Fig. S6 Emission decay profiles of (a) **RuRe(OEt),** (b) **RuRe(Ph)** and (c) **RuRe(FPh)** in CH_3CN, monitored at 620 nm after excitation by a hydrogen discharge lamp with BG12 and KV470 filters (resulting in an excitation wavelength of 460 ~ 500 nm). The corresponding simulated emission intensity changes obtained from the double exponential decay functions are shown as the solid curves. Top panels show the residuals obtained from the simulations.

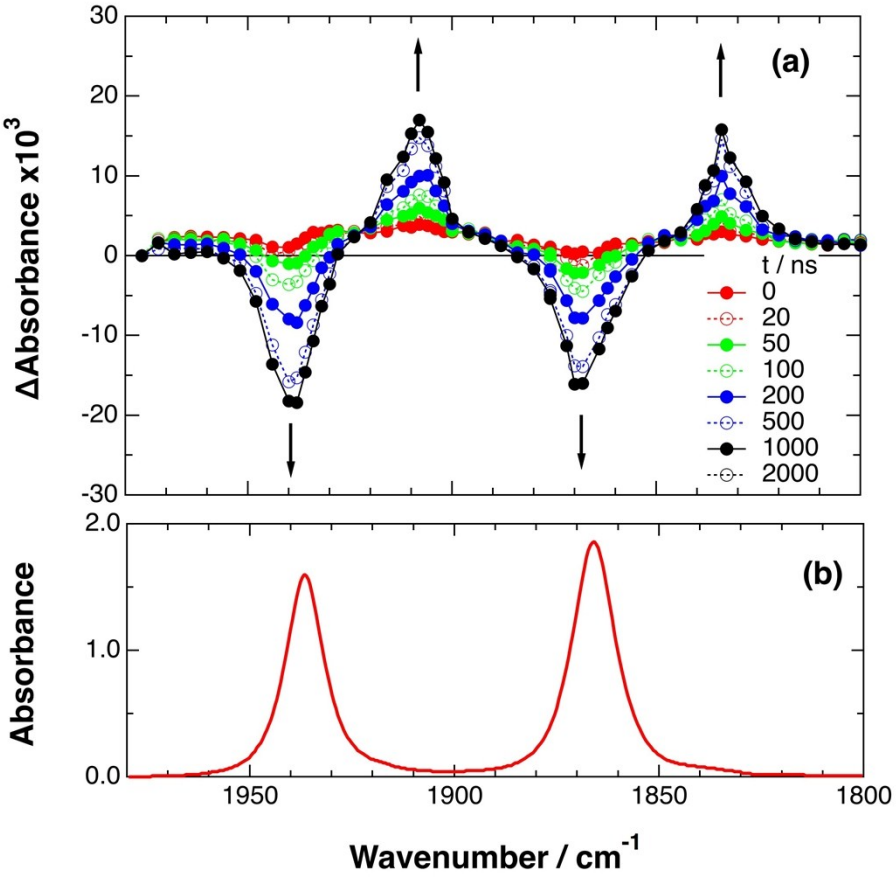

Fig. S7 (a) TRIR spectra recorded after 532 nm excitation of **RuRe(Ph)** (2 mM) in argon-saturated CH_3CN/TEOA (5:1 v/v) containing 0.2 M BNAH. (b) FT-IR spectrum of **RuRe(Ph)** in CH_3CN.

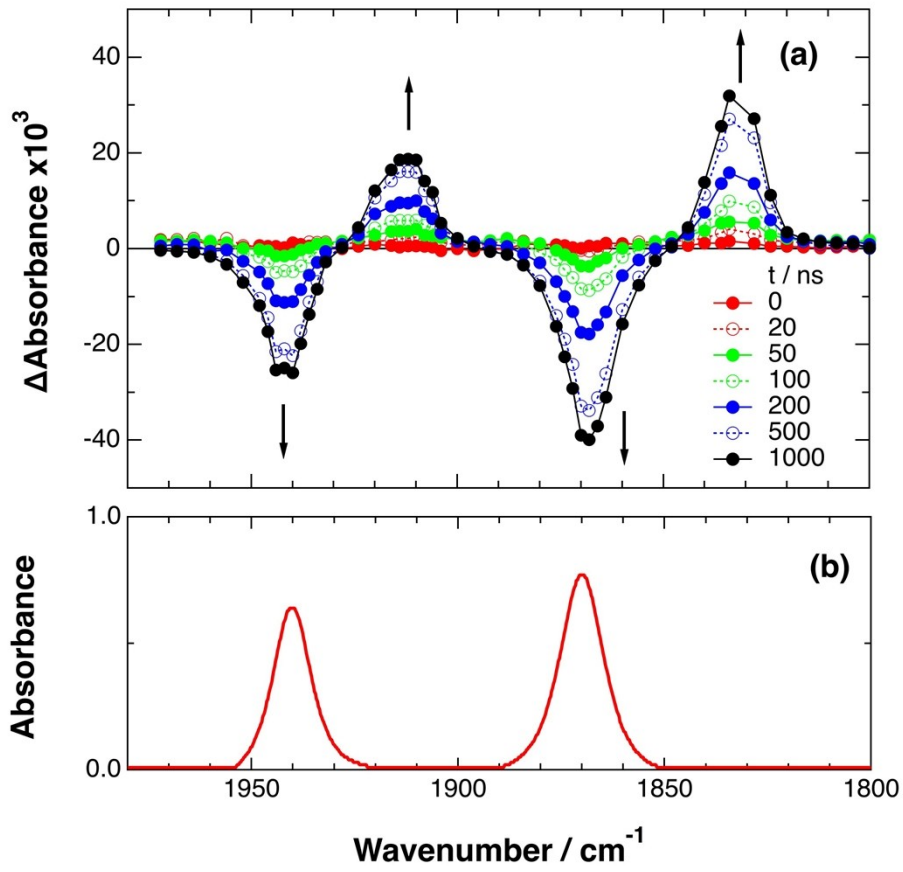

Fig. S8 (a) TRIR spectra recorded after 532 nm excitation of **RuRe(FPh)** (2 mM) in argon-saturated CH_3CN/TEOA (5:1 v/v) containing 0.2 M BNAH. (b) FT-IR spectrum of **RuRe(FPh)** in CH_3CN.

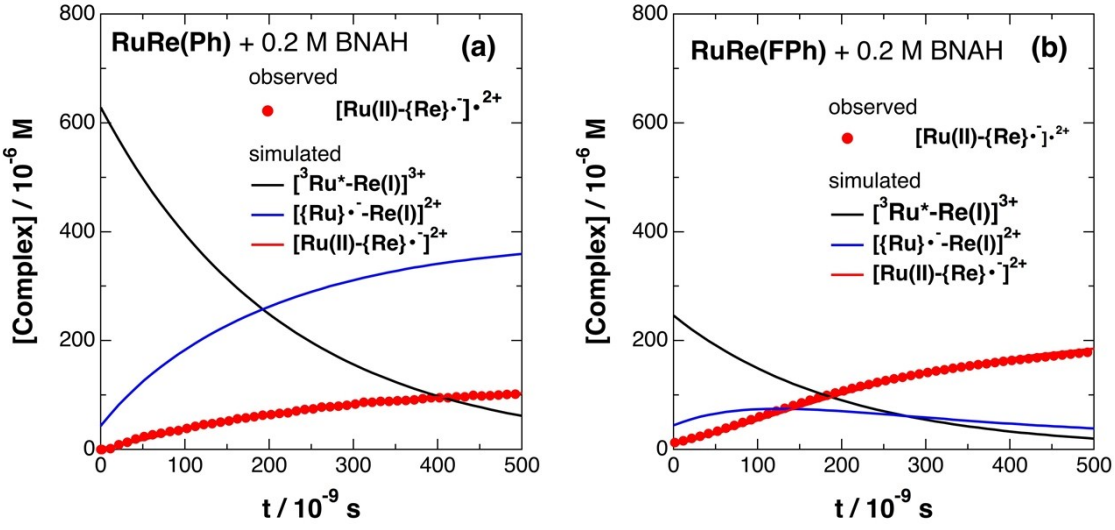

Fig. S9 Time profile of [Ru(II)-{Re}•⁻]²⁺ (•) in the TRIR measurement of (a) **RuRe(Ph)** and (b) **RuRe(FPh)** in the presence of 0.2 M BNAH in an argon-saturated CH_3CN/TEOA (5:1 v/v) solution after 532 nm excitation. The kinetic simulation results for $[^3Ru^*\text{-}Re(I)]^{3+}$, $[\{Ru\}^{\bullet-}\text{-}Re(I)]^{2+}$, and $[Ru(II)\text{-}\{Re\}^{\bullet-}]^{2+}$ are also shown (solid lines).

Emission Spectral Fitting

The 0-0 band energy gaps between the ^{3}MLCT excited state and the ground state ($E_{00}(^3MLCT)$) were obtained from simulation of the emission spectrum by using single-mode Franck-Condon line-shape analysis,[25,26] which was conducted with the Wavemetrics

Igor software. The parameters were optimized by comparison of calculated and experimental spectra by means of the nonlinear least-squares method. Equation S1 was used for the calculated spectra,[26]

$$I(\nu)=\sum_{\nu_m=0}^{5}\left\{\left(\frac{E_{00}-\nu_m h\omega_m}{E_{00}}\right)\left(\frac{S_m{}^{\nu_m}}{\nu_m!}\right)\exp\left[-4\ln 2\left(\frac{\nu-E_{00}+\nu_m h\omega_m}{\Delta\nu_{00,1/2}}\right)^2\right]\right\} \quad \text{(S1)}$$

where the symbols are defined as follows,
$I(\nu)$: the relative emission intensity at frequency ν,
E_{00}: the 0-0 band gap energy,
$h\omega_m$: the average of medium-frequency acceptor modes that are coupled to the electronic transition,
S_m: the electron-vibration coupling constant (Huang-Rhys factor)
$\Delta\nu_{00,1/2}$: the half-width of the 0-0 vibronic band
The sum is taken over the quantum number of the average medium-frequency vibrational mode (ν_m).
The observed and simulated spectra for **RuRe(OEt), RuRe(Ph)**, and **RuRe(FPh)** are shown in Figure S10 and the optimized parameters are summarized in Table S2.

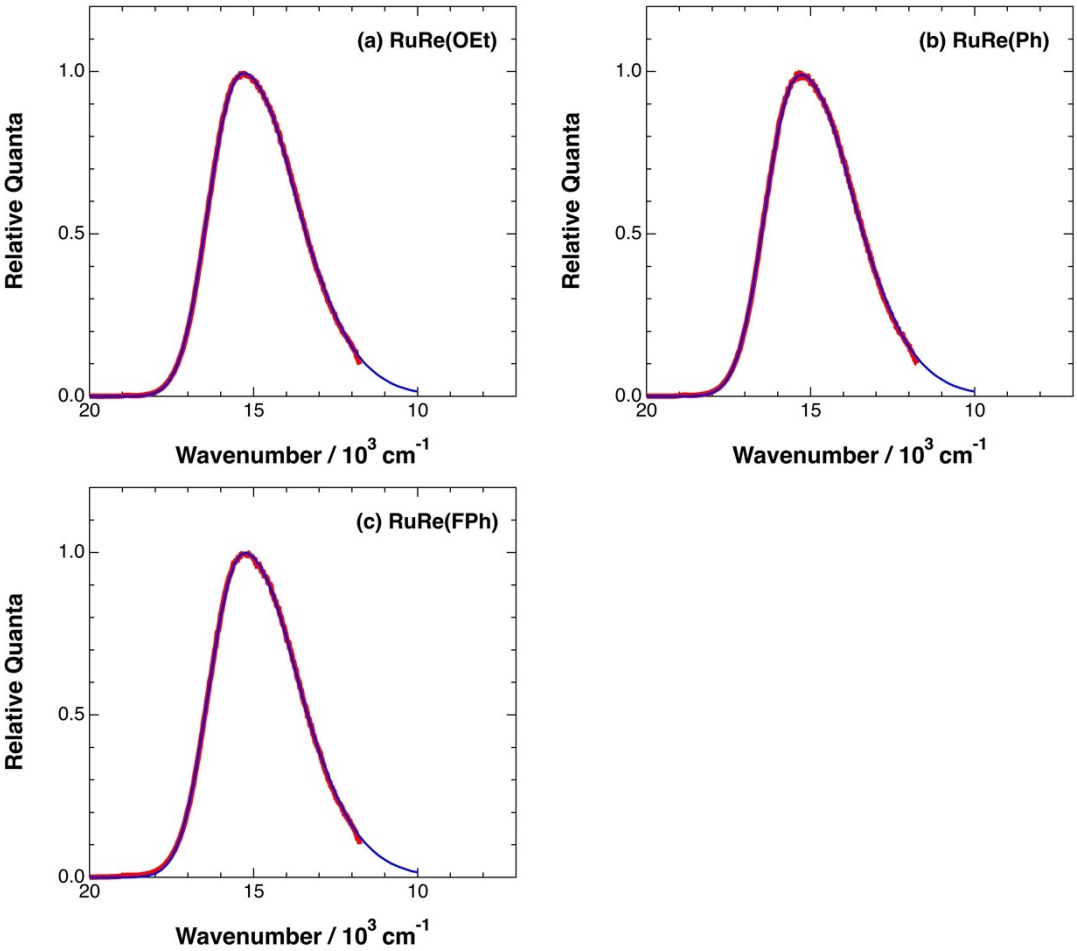

Fig. S10 Observed phosphorescence spectra (red lines) of (a) **RuRe(OEt)**, (b) **RuRe(Ph)** and (c) **RuRe(FPh)** complexes in DMF solutions, excited at 460 nm at 298 K, and spectra simulated by single-mode Frank-Condon analysis (blue lines).[25,26]

Table S1. Evaluated spectral parameters and their 95% confidence intervals for the ^{3}MLCT emission spectral fitting of **RuRe(X)** by using the single-mode Franck-Condon line-shape analysis.

Complex	E_{00} / cm^{-1}	$\Delta\nu_{00,1/2}$ / cm^{-1}	ω_m / cm^{-1}	S_m
RuRe(OEt)	15750 ± 10	1810 ± 10	1320 ± 10	1.05 ± 0.01
RuRe(Ph)	15740 ± 10	1820 ± 10	1320 ± 10	1.04 ± 0.01
RuRe(FPh)	15720 ± 10	1860 ± 10	1330 ± 10	1.03 ± 0.01

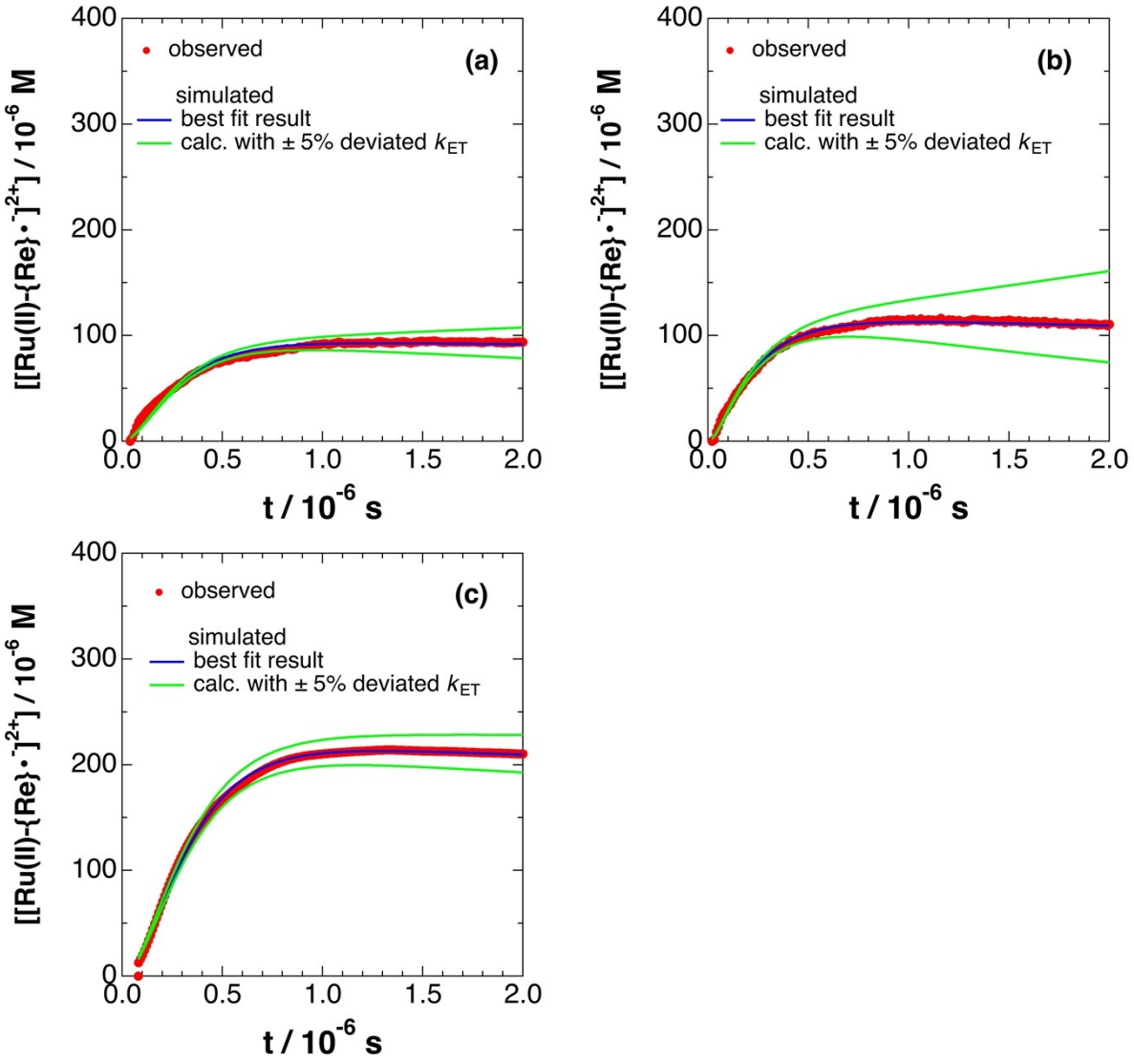

Fig. S11 Observed time profiles of the Re unit OER state ([Ru(II)-{Re}•$^-$]$^{2+}$) (•), the best-fit simulation results (blue solid curves), and the simulation curves calculated with the k_{ET} parameter deviated by ±5% from its best-fit value (green curves) for (a) **RuRe(OEt)**, (b) **RuRe(Ph)**, and (c) **RuRe(FPh)**.

Calculation of the free energy change of the electron transfer from BNAH to the ^{3}MLCT excited state of the Ru unit ([^{3}Ru*-Re(I)]$^{3+}$).

Fukuzumi and coworkers reported the redox potential of BNAH (E^0(BNAH•$^+$/BNAH)) as 0.57 V vs. SCE, i.e., 0.23 V vs. Ag/AgNO$_3$.[31] Therefore, the corresponding free energy change for the reductive quenching of [^{3}Ru*-Re(I)]$^{3+}$ by BNAH can be calculated by using the following equation.[27]

$$-\Delta G_{RQ}{}^0 = -E^0(\text{BNAH}^{\bullet+}/\text{BNAH}) + \{E^0(\text{Ru}^{2+}/\text{Ru}^{+}) + E_{00}(^3\text{Ru}^*)\} + w_p''$$

$$= -(0.23) + (-1.74 + 1.95) + 0.028\{(+1)(+1) - (0)(+2)\} = +0.01 \text{ eV}$$

where the redox potential of **Ru** was used as $E^0(Ru^{2+}/Ru^{+})$. The reason for this was described in the main text.

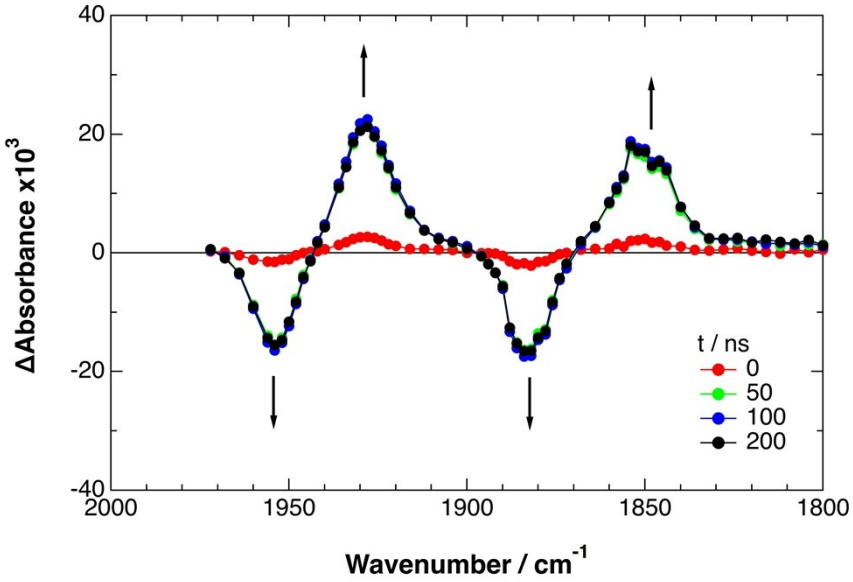

Fig. S12 TRIR spectra recorded after 532 nm excitation of **RuRe(OEt)** (2 mM) in argon-saturated CH_3CN/TEOA (5:1 v/v) containing BIH (0.2 M).

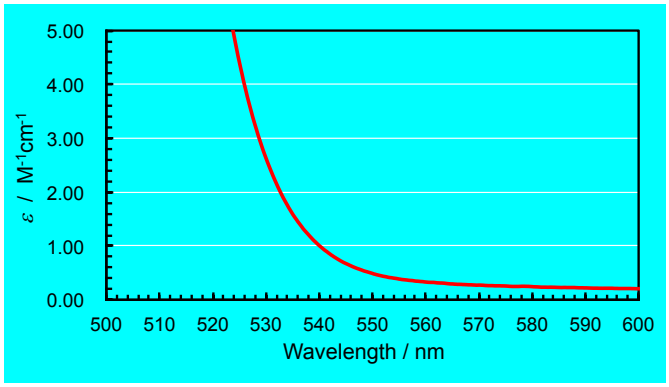

Fig. S13 UV-Vis absorption spectrum of **Re(FPh)** measured in acetonitrile at room temperature.

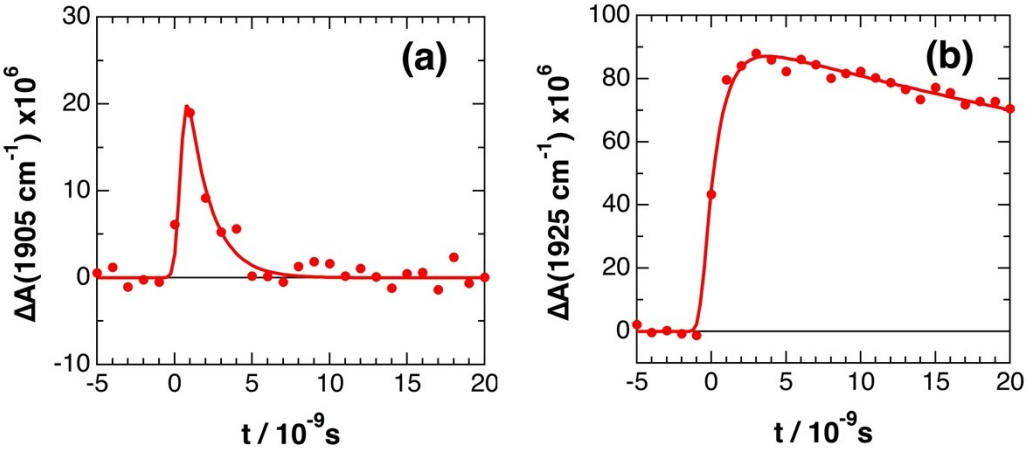

Fig. S14 Decay and growth of the transient infrared absorption bands of **RuRe(FPh)** in CH_3CN, monitored at (a) 1905 cm^{-1} and (b) 1925 cm^{-1}. These plots were fitted as a single-exponential function and a single-exponential rise and decay function with a 600 ps excitation laser pulse duration, respectively, giving (a) τ = 1.5 ± 0.2 ns and (b) τ = 1.1 ± 0.5 ns.

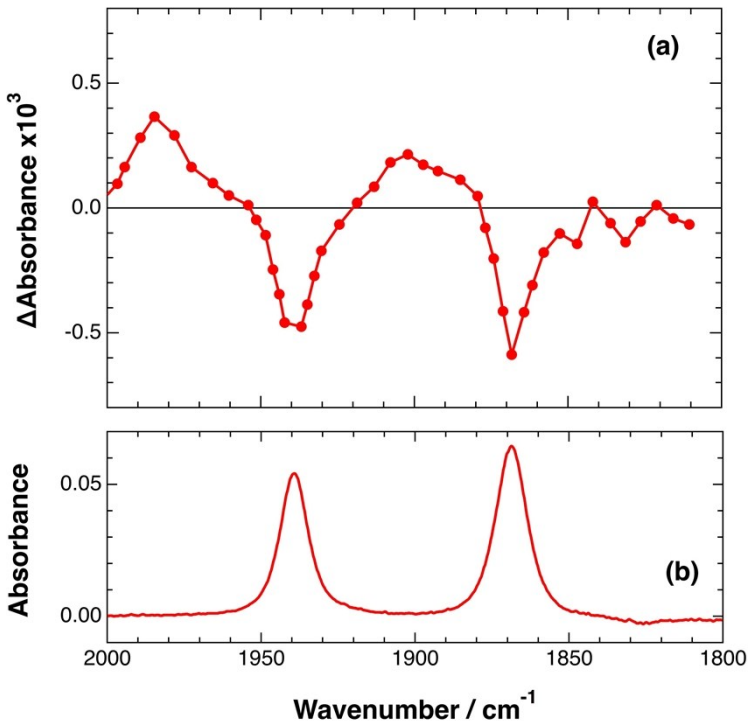

Fig. S15. (a) TRIR spectrum (ps-system) recorded 10 ps after 532 nm excitation of **Re(FPh)** (1 mM) in an argon-saturated CH_3CN solution. (b) FT-IR spectrum of **Re(FPh)** in CH_3CN.